Batteries & Supercaps

Chemistry Europe
European Chemical Societies Publishing

Batteries & Supercaps

RESEARCH ARTICLE OPEN ACCESS

Physics-Based Transmission Line Model for Explanation of Electrochemical Impedance Spectroscopy Spectra of Vanadium-Based Flow Batteries

Sara Drvarič Talian[1] | Thorben Sieling[2] | Ervin Rems[1,3] | Andreas Linhart[2] | Jan Grosse Austing[2] | Jože Moškon[1] | Miran Gaberšček[1,3]

[1]Laboratory for Modern Battery Systems, Department of Materials Chemistry, National Institute of Chemistry, Ljubljana, Slovenia | [2]VANEVO GmbH, Oldenburg, Germany | [3]Faculty of Chemistry and Chemical Technology, University of Ljubljana, Ljubljana, Slovenia

Correspondence: Sara Drvarič Talian (sara.drvarictalian@ki.si)

Received: 7 April 2026 | **Revised:** 21 June 2026 | **Accepted:** 26 June 2026

Keywords: electrical impedance spectroscopy | flow battery | transmission line

ABSTRACT

Existing models describing the impedance response of vanadium flow batteries typically use a bottom-up approach, incrementally adding complexity to simple mathematical descriptions to account for missing transport processes. In this study, we present a reverse, top-down approach by developing a physics-based transmission line model that is general, customizable, and that can be ultimately simplified to a single equation for the studied electrochemical system. The model incorporates transport through the ion-selective membrane, electrolyte-filled pores, and diffusion layer, as well as the reaction at the electrode interface, electronic conductivity of the carbon felt, and contact resistances. This model enables a universal description of flow battery impedance response, which can help identify bottleneck processes and guide improvements in next-generation battery design.

1 | Introduction

Due to their ability to decouple power from capacity, flow batteries are attracting significant attention as promising, scalable energy storage solutions. Among the possible chemistries, vanadium-based flow batteries hold a superior position because the use of vanadium ions as both positive and negative electrolyte components reduces cross-contamination problems [1, 2], decreases degradation compared to other flow battery chemistries [3], and enables the use of less flammable, aqueous electrolytes [4].

Targeted improvements in next-generation battery design require identification of bottleneck processes, which typically demands in-depth analysis of the origins of internal losses during cell operation. Electrochemical impedance spectroscopy (EIS) is a uniquely suited technique for this purpose, as it allows for the decoupling of processes based on their characteristic time scales. In principle, this enables the separation of ohmic resistance, charge–transfer reaction, and diffusional contributions. To connect the physico-chemical processes with the resulting impedance contributions, quantitative modeling of impedance spectra is essential, although approaches vary between analytical solutions [5, 6], numerical methods [7–9], or transmission line models [10–12].

The impedance response of vanadium flow batteries has been systematically studied in the past, notably by Schneider et al. [13], who investigated electrode degradation by deconvoluting EIS spectra using the DRT method (distribution of relaxation times), and by Sun et al. [14], who determined that the negative electrode impedance accounts for roughly 80% of total losses, highlighting significant asymmetry between the two half-reactions. The initial study by Sun et al. was later expanded by the same research group through the implementation of a mathematical model for EIS description [15], which separates

ohmic resistance from charge–transfer reaction and mass-transport losses. This model used a simple de Levie model and enhanced it with a description of diffusional impedance. They showed that the sum of the ohmic, charge–transfer, and finite diffusion overvoltages perfectly matches the applied overpotential and investigated the specific contributions when varying the flow rate or electrode thickness. They demonstrated that diffusion is significantly affected by both the flow rate and the electrode active surface area, while the charge–transfer reaction resistance is influenced by the surface area but not by changes in flow rate. This model was later employed by Pezeshki et al. [16], who modified it to describe the full cell impedance response by summing two single electrode impedances (developed by Sun [15]) with the lead inductance and series resistance.

Importantly, all currently available model descriptions of the impedance response of vanadium flow batteries use a bottom-up approach, starting with a simple model that is incrementally adjusted to attempt to describe the complex electrochemical system. However, these changes mean that the parameters of the final model can lose direct connection to the physical properties and processes of the electrochemical system. This article, however, approaches the problem from a top-down perspective. We propose a general transmission line model to describe the flow battery impedance, which encompasses all proposed transport and faradaic processes that occur in such an electrochemical system. We then demonstrate how this general model can be simplified by neglecting processes that contribute negligible impedance to the specific system under investigation.

2 | Experimental

A single flow battery cell (Pinflow energy storage) with a geometrical active area of $4 \times 5\,cm^2$ was used to record EIS spectra and validate the transmission line model (TLM). Considering the scope of this study, materials are only of secondary importance. The cell was equipped with copper plates (Pinflow energy storage) stacked on commercial bipolar plates serving as current collectors, commercial membranes, and commercial activated carbon felts in flow-through configuration. Membrane 1 was a 30 µm thick anion-exchange membrane and membrane 2 was a 50 µm thick cation-exchange membrane. Both membranes were used without pretreatment. Vanadium electrolyte (1.6 M V, 4 M total sulfate, 70 mM phosphoric acid, AMG TITANIUM - GfE Metalle und Materialien) was used without further purification. Two in-house produced electrolyte reservoirs made of PVC were filled with 80 mL of electrolyte each, which was magnetically stirred and operated under humidified nitrogen (5 N, Linde Gas). A peristaltic pump (Watson-Marlow 323Du) and Marprene tubes (Watson-Marlow) were used to transport electrolyte. The whole setup was placed in a climate chamber (MKB 300, Flohr Instruments) set to 30°C. After final assembly, the setup was left with pumped electrolyte for 1–2 h to equilibrate in the climate chamber prior to starting experiments.

An Interface 5000E potentiostat (Gamry Instruments) was used for electrochemical characterization. Cables were twisted and directed to reduce inductance [17]. EIS spectra were measured in galvanostatic mode at open circuit voltage with 6 points per decade, at 500 kHz–30 mHz, and an amplitude of 0.1 A rms (geometrical $5\,mA/cm^2$ rms). Unless otherwise specified, a flow rate of $47\,mL\,min^{-1}$ and a SoC of 0.5 were used. For testing and validating different conditions, flow rates and SoCs were varied to 19, 47, and $85\,mL\,min^{-1}$ (setup with membrane 1) and 0.017, 0.495, and 0.940 (setup with membrane 2), respectively. Spectra recorded directly after first acquisition showed negligible drift effects in the diffusion region.

Impedance spectra were simulated using custom Python 3 code with standard scientific packages (Matplotlib and NumPy). The code was based on the mesh method for solving planar electrical circuits, as described elsewhere [18, 19]. The electrical circuit construction is described in the next chapter.

2.1 | Transmission Line Model

In the current transmission line model, we assume the following electrochemical cell construction: a porous carbon electrode is placed on top of a nonporous carbon current collector. The electrode pores are filled with electrolyte containing the electroactive species. On the opposite side, the electrode is in contact with an ion-selective membrane. On the other side of the membrane, the second half cell is comprised of similar components with a different chemical composition of the electrolyte. We assume that the concentration of electroactive species in the bulk of the carbon electrode pore is maintained at a constant level by an external pump, since the EIS measurement does not change the state of charge (SOC) significantly. Next to the electrode surface, a diffusion layer forms, where the electroactive species diffuse between the bulk of the electrode pore (where the species' concentration is constant) and the carbon surface. On the carbon surface, the electroactive species (i.e., vanadium ions, protons) undergo a redox reaction (Equations I and II).

$$\text{Negative half-cell} \qquad V^{2+} \rightleftharpoons V^{3+} + e^- \tag{I}$$

$$\text{Positive half-cell} \qquad VO_2^+ + 2H^+ + e^- \rightleftharpoons VO^{2+} + H_2O \tag{II}$$

The inactive ions contribute to the formation of a double layer. Electrons reach this point through the electronically conductive fibers of the carbon felt electrode. The electrons enter the carbon felt through its contact with the current collector. On the other side, the ion-selective membrane in contact with the carbon allows the transport of charge-balancing protons and/or sulfate/bisulfate ions, depending on whether a cation- or an anion-exchange membrane is used. Note that this assumes an ideal ion-selective membrane, which is here modeled by assuming a large value for element Z_{13}. If the ion-selective membrane is not ideal, the said model parameter can be adjusted to smaller values to allow for membrane "leakage."

With this description of the internal processes in mind, we built a circuit for the transmission line model (Figure 1). In the scheme, the elements of the electrochemical flow battery cell are shown as shaded areas (current collector, carbon felt, diffusion layer, carbon felt pore filled with electrolyte, and ion-selective membrane). Within these shaded areas, the circuit describes the electronic and ionic rails with the impedance elements drawn and

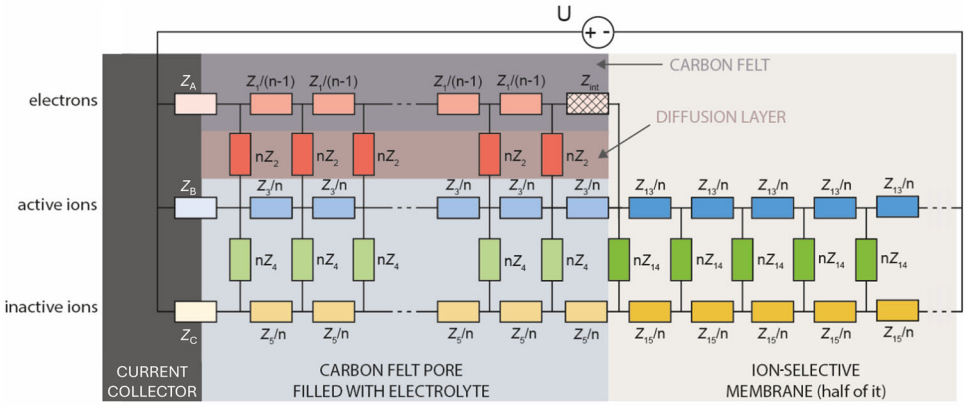

FIGURE 1 | Scheme of the transmission line model equivalent circuit for a carbon felt electrode in a flow battery half-cell.

connected as described in the previous paragraph. The contributions of the other half-cell are a mirror circuit on the right-hand side of Figure 1.

Depending on the relative values of the elements for each half-cell, one half-cell can dominate the impedance response or the contributions of both can be of similar values. For the presented case, we limited the model to processes occurring at the negative electrode, which likely accounts for about 80% of the total cell impedance [14]. With this selection, we reduced the number of unknown parameters to less than 50%, as we could avoid additional complications from proton transport that must be included at the positive electrode. Typical values and meanings of the impedance elements are summarized in Table 1. Despite this simplified description, we still captured the main trends in the EIS spectra during systematic variation of the experimental conditions, as shown in the Experimental validation of the TLM section. In the case that one electrode does not dominate the impedance response and the simulation of both half-cells is required, the model can be easily adapted. Nevertheless, such spectra usually exhibit significant overlap of features and distorted arcs, which complicates the determination of circuit element values. Dedicated three-electrode measurements or symmetrical cell measurements are therefore needed to first determine the range of values for the parameters pertaining to the positive or negative half-cell. Only after those experiments are conducted can the full-cell response be understood.

In a typical spectrum simulated with such a model (Figure 2), we see several contributions with their shapes, resistance, and capacitance values controlled by a relatively small number of parameters. The parameter values for this simulation were assumed but kept in close range to typical values from Table 1. From high to low frequency, these are:

- Resistive intercept, which depends on the ion-selective membrane (R_{15}). This contribution also depends on the contact resistance (R_A), but we used a negligibly small value for the contact resistance in the present simulations.
- Inductive contribution due to wiring, which depends on the cable inductance (L)
- A nonsymmetrical charge–transfer resistance arc, which depends on the electronic resistance of the carbon felt (R_E), charge transfer reaction resistance (R_{CT}), and the double-layer capacitance (C_{dl}). The asymmetry originates from the limited electronic conductivity of the carbon felt. This phenomenon is well known from simpler transmission lines based on the de Levie model. Specifically, the asymmetry (tailing) occurs because the signal experiences a distributed resistance as electrons migrate deeper into the pore, while simultaneously being consumed by the interfacial capacitance/reaction along the pore walls.
- Low frequency arc due to diffusion in the thin diffusional layer next to the electrode, which depends on Warburg resistance (R_W) and capacitance (C_W).

2.2 | Experimental Validation of the TLM

This model was validated by examining the effects of several cell design changes on the impedance spectrum and comparing the results to measured impedance spectra. The effects of ion-selective membrane type, flow rate, and SOC were investigated. Only half of the cell is included in the model, effectively modeling the impedance response of one electrode. In contrast, the EIS measurements were conducted on full cells due to laboratory limitations. The model can be readily adapted to this by adding a mirror circuit on the right-hand side of the circuit shown in Figure 1 and adjusting the values of the elements for the newly added electrode. However, we did not use this approach to avoid overparameterizing the origins of the spectral differences, since previous studies have already shown the prevalence of the negative electrode impedance [14]. It should be noted that this means we neglect a possible origin of the asymmetry in the charge–transfer resistance arc, which could result from differences in parameters associated with oxidation at one electrode and reduction at the other.

The effect of the ion-selective membrane was investigated by keeping the cell design constant except for changing the type of ion-selective membrane separating the electrodes. The measured spectra show a shift in the resistive intercept and a constant peak frequency of both impedance arcs, while the resistance of the arcs changes only slightly (Figure 3a,b). According to the TLM model, changing the ion-selective membrane type should only change the value of R_{15}, which affects the resistive intercept, while keeping the

TABLE 1 | List of impedance elements employed in the TLM from Figure 1, with their formula, physical meaning, and typical values. In order to increase the accuracy of the description of experimental spectra, we replaced the double-layer capacitance with an appropriate constant phase element (CPE), assuming the exponent α in the range of 0.90–0.95.

Impedance element	Element formula in present model	Physical meaning of elements in formula	Typical values for present setup
Z_A	R_A	Electronic contact resistance between current collector and carbon felt	To not over-parametrize the model, we assume a negligible contact resistance
Z_B	$1/(j\omega\ C_B)$	Double layer capacitance (interaction of active ions with the current collector)	Negligible capacitance due to small surface area they are associated with
Z_C	$1/(j\omega\ C_C)$	Double layer capacitance (interaction of inactive ions with the current collector)	Negligible capacitance due to small surface area they are associated with
Z_1	R_E	Electron resistance of carbon felt	8 mΩ experimentally determined[a]
Z_2	$((R_{CT}+Z_W)^{-1}+1j\omega\ C_{dl})^{-1}$, where $Z_W = R_W * (R_W * 1j\omega\ C_W)^{-0.5}$ *tanh$(R_W * 1j\omega\ C_W)^{0.5}$	Diffusion of active ions in the diffusional layer and their charge transfer reaction on the carbon felt surface, coupled with double layer capacitance	C_{dl} is 10^{-6}–10^{-5} F per cm^2 of electrode active area [20, 21] C_W is a few kF
Z_3	R_3	Migration resistance of active ions in carbon felt pore	Negligible resistance due to external pump keeping the concentration of ions in the bulk of the pore constant
Z_4	$1/(j\omega\ C_{chem,\ 4})$	Chemical capacitance due to diffusion in carbon felt pore	Large capacitance due to external pump keeping the concentration of ions in the bulk of the pore constant
Z_5	R_5	Migration resistance of supporting electrolyte in carbon felt pore	Negligible resistance due to external pump keeping the concentration of ions in the bulk of the pore constant
Z_{int}	$1/(j\omega\ C_{int})$	Double layer capacitance formed on the interface between the ion-selective membrane and carbon felt	Negligible capacitance
Z_{13}	R_{13}	Migration resistance of active ions in ion-selective membrane	Large resistance (assumed ideal ion-selective membrane)
Z_{14}	$1/(j\omega\ C_{chem,\ 14})$	Chemical capacitance due to diffusion in ion-selective membrane	Irrelevant for the frequency range we are exploring
Z_{15}	R_{15}	Migration resistance of supporting electrolyte in ion-selective membrane	A few mΩ
Z_L	$J\omega\ L$	Inductance of cables	$L = 10^{-6}$–10^{-8} H [22, 23]

[a]Note that the electronic resistance of the carbon felt was experimentally determined to be 8 mΩ for the electrode size used (4×5 cm^2). This value was obtained using a four-probe measurement on five different dry electrode lengths, assuming that the electronic conductivity of the carbon felt is the same across and along its surface. Since the fibers of the felt run alongside the measured surface, we assume that the electrical conductivity might be smaller if measured across, which means that the value obtained is the lower limit for its resistance (or upper limit for electrical conductivity).

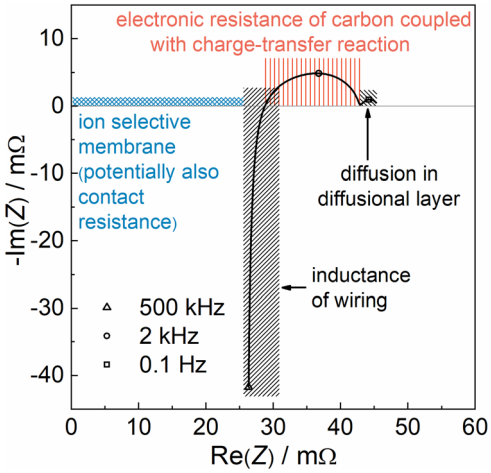

FIGURE 2 | A typical impedance spectrum simulated using the transmission line model from Figure 1. The values of the parameters were the following: $R_{15} = 2.5 \cdot 10^{-2}\,\Omega$, $L = 1.3 \cdot 10^{-7}\,\mathrm{H}$, $R_E = 1.5 \cdot 10^{-2}\,\Omega$, $R_{CT} = 1.1 \cdot 10^{-3}\,\Omega$, $C_{dl} = 6.5 \cdot 10^{-2}\,\mathrm{F}$, $R_W = 1.2 \cdot 10^{-3}\,\Omega$, $C_W = 3.7 \cdot 10^{3}\,\mathrm{F}$. Blue and red colors indicate the largest contributions in the impedance spectrum, which account for most of the internal resistance of the electrochemical cell.

high-frequency and low-frequency arcs constant (Figure 3c,d). Although we would therefore expect stable resistances of both arcs in the measurements, it should be noted that the variations in arc resistance in Figure 3a,b are within the margin of error for repeated measurements, suggesting that the transmission line model successfully describes the expected differences resulting from the change in ion-selective membrane.

The effect of the change in flow rate was investigated by increasing the flow rate from 19 to 47 mL min^{-1} and finally to 85 mL min^{-1} in a single cell measurement setup. For this set of measurements, we observed practically constant values for the resistive intercept and high-frequency arc, while the diffusional resistance contribution and associated peak frequency varied with the flow rate. The former increases with a decrease in flow rate, while the peak frequency decreases in the same direction (Figure 4a,b).

Higher flow rates decrease the Warburg resistance and increase the peak frequency of the diffusional arc due to a decrease in the thickness of the diffusional layer. In order to simulate this correlation, we compare the analytical correlation between the average diffusion layer thickness δ_{avg} and volume flow rate Q of a simple flat electrode model system (see Appendix A) to the proposed empirical relations describing real felt electrodes. Although the flat electrode approximation oversimplifies the treatment of real (porous) felt electrodes, the correlation in Equation (1) still provides a fair illustration of the δ_{avg}–Q relationship for the employed system.

$$\delta_{avg} \propto Q^{-\frac{1}{3}} \tag{1}$$

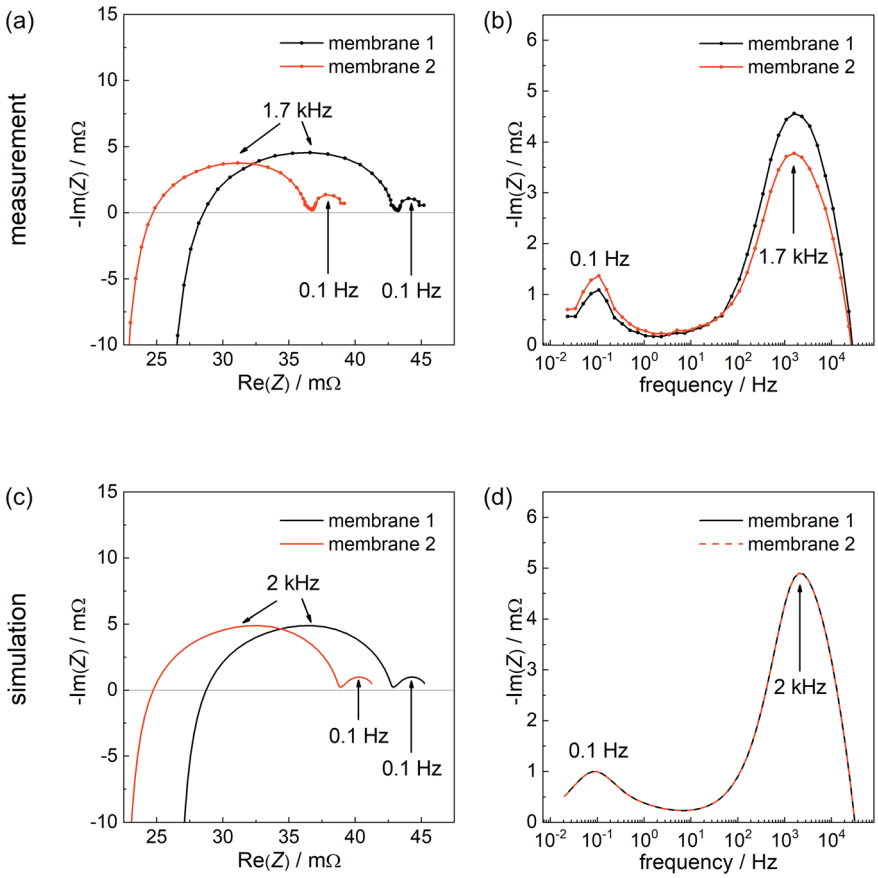

FIGURE 3 | Nyquist plots (a, c) and imaginary parts of Bode plots (b, d) of impedance spectra for measurements (top row) and simulations (bottom row) when changing the ion-selective membrane.

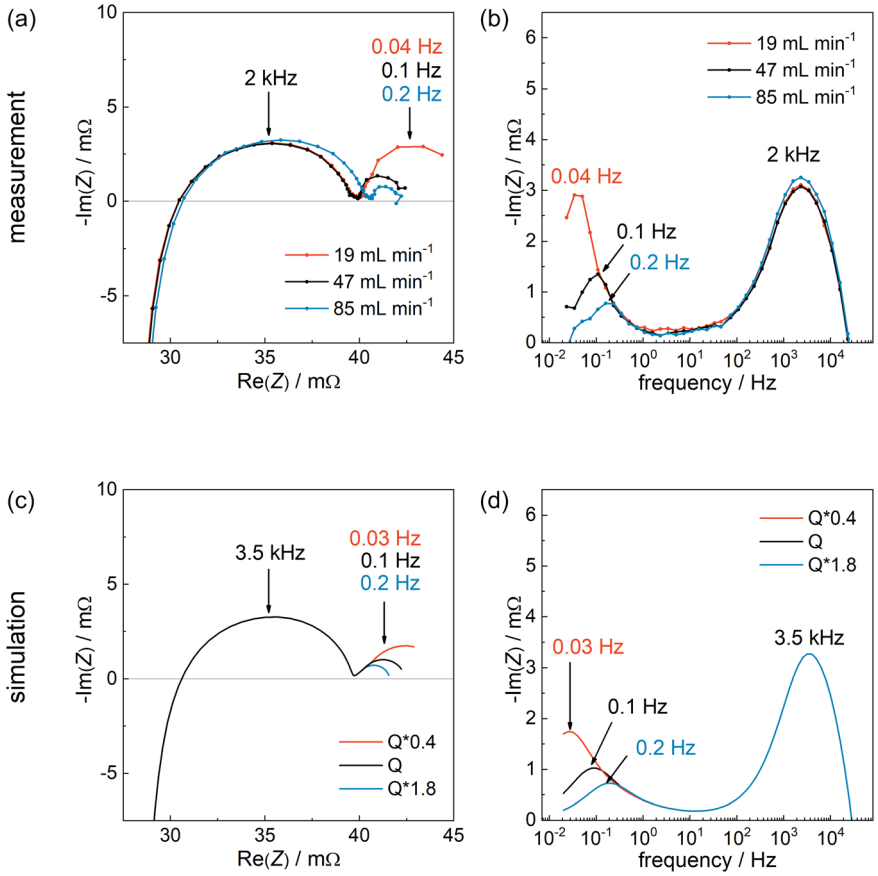

FIGURE 4 | Nyquist plots (a, c) and imaginary parts of Bode plots (b, d) of impedance spectra for measurements (top row) and simulations (bottom row) when changing the flow rate.

Indeed, numerous experimental studies using porous felt electrodes suggest that the $\delta_{avg}-Q$ relation can be described by empirical correlations where the average Nernst diffusion layer thickness, δ_{avg}, can be expressed by:

$$\delta_{avg} = \frac{d_f}{Sh} \tag{2}$$

where d_f is the fiber diameter and Sh is the Sherwood number. The latter is in general expressed as a function of the Reynolds number (Re) and the Schmidt number (Sc) (see Appendix B):

$$Sh = a Re^b Sc^c \tag{3}$$

with a prefactor a and exponents b and c. Since Re is proportional to the mean velocity $\overline{u}$ (Appendix B), δ_{avg} is dependent upon Q^{-b} (Equation (4)).

$$\delta_{avg} \propto Q^{-b} \tag{4}$$

Whereas the exponent in the flat electrode approach of Equation (1) is fixed to $b = 1/3$, the exponent in Equation (4) is related to parameterization of Re. In different studies various values of b were obtained, typically ranging between the flat electrode approximation of 1/3 (0.35 and 0.4) [24], 0.66 [25], up to much larger values reported in some studies (0.9) [26], approaching the upper bound value of 1 predicted for ideal microchannel electrode geometry [27]. To determine the best value of exponent b for our experimental data, the peak frequency and arc resistance for the low frequency impedance arc were extracted from the experimental spectra for all three tested flow rates. The data were then fitted to the following relationships:

$$f = k_f Q^{2b} \tag{5a}$$

$$R_W = k_R Q^{-b} \tag{5b}$$

where f denotes the Warburg peak frequency, R_W the Warburg arc resistance, and k_f and k_R the corresponding pre-exponential factors. The relations were linearized and the best-fit model was obtained by minimizing a least squares objective function (Equation (6)), resulting in $b = 0.61$. In Equation (6), f and R_W were expressed in Hz and mΩ, respectively, to ensure that comparable scale of ln f and ln R_W values.

$$\min_{b,k_f,k_R} \left(\sum_{i=1}^{3} \left(\ln f_i - \left(\ln k_f + 2b \ln Q_i \right) \right)^2 + \sum_{i=1}^{3} \left(\ln R_{W,i} - \left(\ln k_R - b \ln Q_i \right) \right)^2 \right) \tag{6}$$

Since both the Warburg resistance (R_W) and capacitance (C_W) parameters linearly increase with the diffusion layer thickness, the correlation in Equation (4) was used to adjust the R_W and C_W. From the median flow rate (47 mL min^{-1}), the flow was either decreased for a factor of 0.4 (19 mL min^{-1}) or increased for a factor of 1.8 (85 mL min^{-1}). Consequently, R_W and C_W parameters were adjusted by factors of 1.75 ($0.4^{-0.61}$, 19 mL min^{-1}) or 0.70 ($1.8^{-0.61}$, 85 mL min^{-1}). The simulated

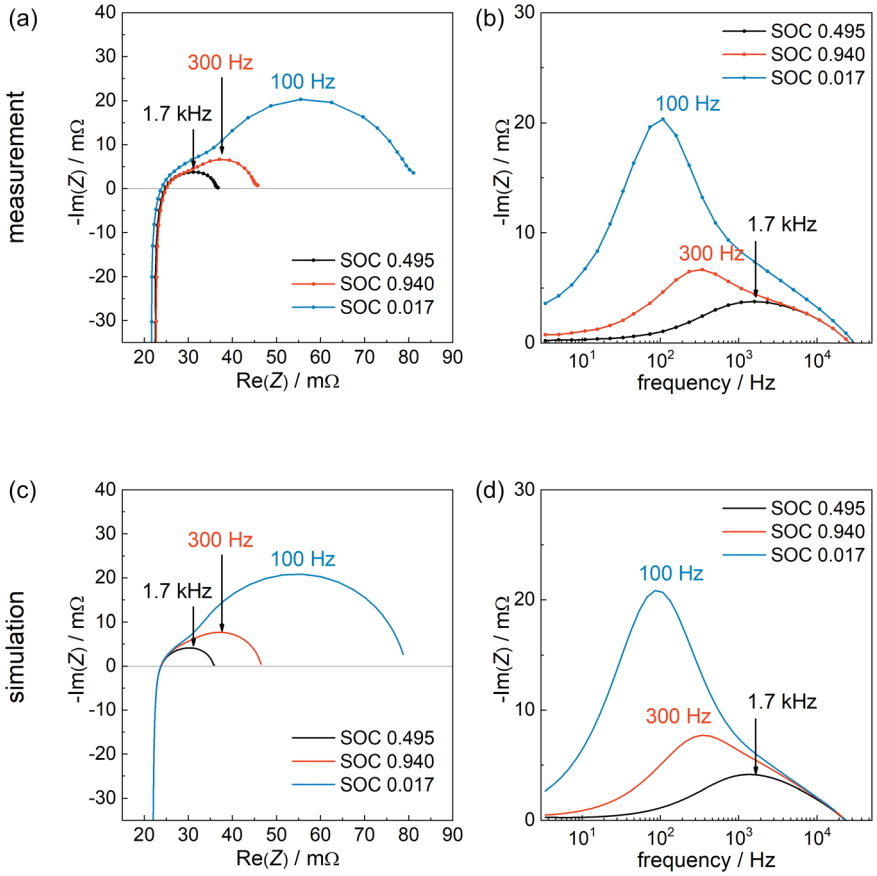

FIGURE 5 | Nyquist plots (a, c) and imaginary parts of Bode plots (b, d) of impedance spectra for measurements (top row) and simulations (bottom row) when changing SOC.

impedance spectra show changes only in the low frequency Warburg contribution, with a decrease in resistance and decrease in peak frequency with an increase in flow rate (Figure 4c,d). The proposed model enables good prediction of the observed changes in the low-frequency contribution, while keeping the resistive intercept and the charge transfer reaction impedance arc the same.

Change in SOC affects the impedance spectrum by altering the shape and size of the high-frequency arc, which becomes increasingly nonsymmetrical as the SOC decreases, showing two distinct contributions with approximately a 20-fold difference in characteristic time constant (Figure 5a,b). The faster process remains in a similar position, consistent with the assumption that this contribution is due to the electrical conductivity of the felt, as we do not expect changes in its value. Assignment of the faster process to distributed resistance is in line with findings of double half-cell experiments [3, 13, 14, 16]. According to the model, changes in SOC are expected to change the values of charge–transfer resistance (R_{CT}), which introduces variations in the high-frequency arc while other differences are negligible. In the model simulations, R_{CT} was adjusted so that the values correlate with experimental data. As R_{CT} is proportional to concentrations of both reduced and oxidized forms of active species, lowest R_{CT} is expected at SOC = 0.5, and R_{CT} should increase when deviating to more extreme SOCs. Assuming constant non-negligible electrical conductivity of the carbon felt produces simulated impedance spectra, which are well correlated with the cell impedance measurements (Figure 5c,d). Overall, the agreement between experimental data and simulations suggests that the present model is valid in at least the SOC range of 0.017–0.940.

With these investigations we have therefore confirmed that the present model is robust enough to describe the impedance spectra sufficiently well for a range of cell conditions spanning different membrane types, flow rates and SOCs. The use of the model nevertheless necessitates a computationally more expensive approach than commonly desired in the experimental field, especially if it is adapted to fitting of experimental data. Interestingly, the proposed transmission line model can be simplified due to the negligible values of certain elements (in particular, Z_3 and Z_5; see Table 1), which allows for a closed-form analytical expression to be derived for the total impedance response. We show the approach and validate it in the next chapter.

2.3 | Simplification of the TLM

For this purpose, the rails in the "carbon felt pore filled with electrolyte" are simplified to a single rail without elements. Additionally, the rails in the ion-selective membrane are reduced to a single Z_{15} element. This results in a de Levie type of transmission line (Figure 6a), which relates to the general solution for the impedance response of a planar electrochemical cell involving four terminals [28]. Impedance of this circuit equals and can be simulated using Equation (7), where $g = \sqrt{Z_1/Z_2}$.

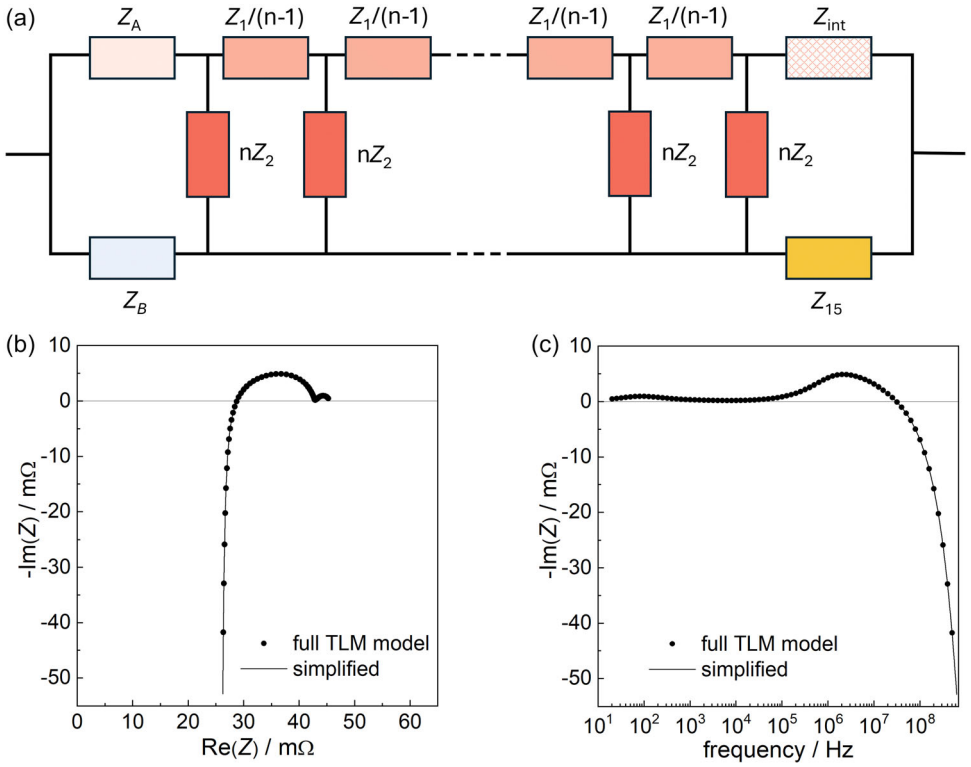

FIGURE 6 | (a) Simplified equivalent circuit describing the flow battery electrode impedance response. Parameter meanings are the same as in Figure 1 and Table 1. (b and c) Comparison of spectra simulated with the full and simplified models shown on a Nyquist plot and the imaginary part of the Bode plot, respectively.

$$Z_{\text{simplified}} = \frac{\begin{array}{l}-2Z_1Z_BZ_{15} + Z_1(Z_A(Z_B+Z_{15}) + Z_BZ_{15} + 2Z_BZ_{15} + Z_{int}Z_{15})\cosh g + \\ +g(Z_1Z_2(Z_B+Z_{15}) + Z_AZ_B(Z_{int}+Z_{15}) + Z_AZ_{int}Z_{15} + Z_BZ_{int}Z_{15})\sinh g\end{array}}{Z_1(Z_A+Z_B+Z_{int}+Z_{15})\cosh g + g(Z_1Z_2 + (Z_A+Z_B)(Z_{int}+Z_{15}))\sinh g} \quad (7)$$

Using Equation (2), we simulated the impedance spectra and compared it to the full transmission line model from Figure 1. The resulting impedances match perfectly (Figure 6b,c), validating the approach. This simplified circuit therefore yields a single governing equation that retains the essential physicochemical interpretation of the full model while being more practical for experimental use.

3 | Conclusions

In this study, we developed a transmission line model to characterize the impedance spectra of vanadium flow batteries. The framework demonstrates broad applicability to various flow battery chemistries. We validated the model by establishing a strong correlation between experimental observations and simulated trends under systematically varied conditions, including membrane type, electrolyte flow rate, and SOC. The proposed model is highly versatile; it can be configured to simulate either full-cell or single-electrode responses and is amenable to model reduction by neglecting insignificant impedance contributions. This capability was demonstrated by reducing the general framework to a de Levie-type transmission line for the system under investigation. Finally, we provided an analytical solution for this simplified case to facilitate its straightforward implementation in future research.

Author Contributions

Sara Drvarič Talian: conceptualization, methodology, software, validation, formal analysis, writing – original draft, writing – review and editing, visualization, funding acquisition. **Thorben Sieling**: conceptualization, investigation, data curation, writing – original draft, writing – review and editing. **Ervin Rems**: software. **Andreas Linhart**: funding acquisition, project administration. **Jan Grosse Austing**: supervision. **Jože Moškon**: conceptualization. **Miran Gaberšček**: methodology, software, writing – original draft, funding acquisition.

Acknowledgments

The authors acknowledge funding from European Union's Horizon Europe research and innovation programme project BatCAT (grant agreement No 101137725). Additionally, S.D.T acknowledges funding from the Slovenian Research and Innovation Agency through core program funding P2_0423.

Funding

This study was supported by European Commission (101137725); Javna Agencija za Raziskovalno Dejavnost RS (P2_0423).

Conflicts of Interest

The authors declares no conflicts of interest.

Data Availability Statement

The data that support the findings of this study are available from the corresponding author upon reasonable request.

References

1. M. Skyllas-Kazacos, L. Cao, M. Kazacos, N. Kausar, and A. Mousa, "Vanadium Electrolyte Studies for the Vanadium Redox Battery—A Review," *ChemSusChem* 9 (2016): 1521–1543.

2. M. Ulaganathan, V. Aravindan, Q. Yan, S. Madhavi, M. Skyllas-Kazacos, and T. M. Lim, "Recent Advancements in All-Vanadium Redox Flow Batteries," *Advanced Materials Interfaces* 3 (2016): 1500309.

3. H. R. Jiang, J. Sun, L. Wei, M. C. Wu, W. Shyy, and T. S. Zhao, "A High Power Density and Long Cycle Life Vanadium Redox Flow Battery," *Energy Storage Materials* 24 (2020): 529–540.

4. A. H. Whitehead, T. J. Rabbow, M. Trampert, and P. Pokorny, "Critical Safety Features of the Vanadium Redox Flow Battery," *Journal of Power Sources* 351 (2017): 1–7.

5. G. Sikha and R. E. White, "Analytical Expression for the Impedance Response of an Insertion Electrode Cell," *Journal of the Electrochemical Society* 154 (2007): A43.

6. J. Huang and J. Zhang, "Theory of Impedance Response of Porous Electrodes: Simplifications, Inhomogeneities, Non-Stationarities and Applications," *Journal of the Electrochemical Society* 163 (2016): A1983–A2000.

7. A. Shodiev, E. N. Primo, M. Chouchane, et al., "4D-Resolved Physical Model for Electrochemical Impedance Spectroscopy of $Li(Ni_{1-x-}yMnxCo_y)O_2$-Based Cathodes in Symmetric Cells: Consequences in Tortuosity Calculations," *Journal of Power Sources* 454 (2020): 227871.

8. A. Shodiev, M. Chouchane, M. Gaberscek, et al., "Deconvoluting the Benefits of Porosity Distribution in Layered Electrodes on the Electrochemical Performance of Li-Ion Batteries," *Energy Storage Materials* 47 (2022): 462–471.

9. A. Alhammadi, A. Fetyan, R. A. Susantyoko, I. Mustafa, and M. O. Bamgbopa, "Understanding Characteristic Electrochemical Impedance Spectral Data of Redox Flow Batteries with Multiphysics Modeling," *Journal of Energy Chemistry* 102 (2025): 329–339.

10. J. Moškon, J. Žuntar, S. D. Talian, R. Dominko, and M. Gaberšček, "A Powerful Transmission Line Model for Analysis of Impedance of Insertion Battery Cells: A Case Study on the NMC-Li System," *Journal of the Electrochemical Society* 167 (2020): 140539.

11. K. Zelič, T. Katrašnik, and M. Gaberšček, "Derivation of Transmission Line Model from the Concentrated Solution Theory (CST) for Porous Electrodes," *Journal of the Electrochemical Society* 168 (2021): 070543.

12. J. Jamnik and J. Maier, "Generalised Equivalent Circuits for Mass and Charge Transport: Chemical Capacitance and Its Implications," *Physical Chemistry Chemical Physics* 3 (2001): 1668–1678.

13. J. Schneider, T. Tichter, P. Khadke, R. Zeis, and C. Roth, "Deconvolution of Electrochemical Impedance Data for the Monitoring of Electrode Degradation in VRFB," *Electrochimica Acta* 336 (2020): 135510.

14. C.-N. Sun, F. M. Delnick, D. S. Aaron, A. B. Papandrew, M. M. Mench, and T. A. Zawodzinski, "Probing Electrode Losses in All-Vanadium Redox Flow Batteries with Impedance Spectroscopy," *ECS Electrochemistry Letters* 2 (2013): A43–A45.

15. C.-N. Sun, F. M. Delnick, D. S. Aaron, A. B. Papandrew, M. M. Mench, and T. A. Zawodzinski, "Resolving Losses at the Negative Electrode in All-Vanadium Redox Flow Batteries Using Electrochemical Impedance Spectroscopy," *Journal of the Electrochemical Society* 161 (2014): A981–A988.

16. A. M. Pezeshki, R. L. Sacci, F. M. Delnick, D. S. Aaron, and M. M. Mench, "Elucidating Effects of Cell Architecture, Electrode Material, and Solution Composition on Overpotentials in Redox Flow Batteries," *Electrochimica Acta* 229 (2017): 261–270.

17. Gamry Instruments Inc. (2016), https://www.gamry.com/assets/Uploads/EIS-on-Very-Low-Z-Battery.pdf.

18. S. D. Talian, J. Bobnar, A. R. Sinigoj, I. Humar, and M. Gaberšček, "Transmission Line Model for Description of the Impedance Response of Li Electrodes with Dendritic Growth," *Journal of Physical Chemistry C* 123 (2019): 27997–28007.

19. S. D. Talian, J. Moškon, R. Dominko, and M. Gaberšček, "Impedance Response of Porous Carbon Cathodes in Polysulfide Redox System," *Electrochimica Acta* 302 (2019): 169–179.

20. M. Schalenbach, V. Selmert, A. Kretzschmar, et al., "How Microstructures, Oxide Layers, and Charge Transfer Reactions Influence Double Layer Capacitances. Part 1: Impedance Spectroscopy and Cyclic Voltammetry to Estimate Electrochemically Active Surface Areas (ECSAs)," *Physical Chemistry Chemical Physics* 26 (2024): 14288–14304.

21. R. Nigam and K. K. Kar, "Simulation Study of Electric Double-Layer Capacitance of Ordered Carbon Electrodes," *Langmuir* 38 (2022): 12235–12247.

22. S. Cruz-Manzo, "Further Understanding of Uncertainties in the Impedance Spectrum of the Polymer Electrolyte Fuel Cell Due to Inductive Effects and Oxygen Diffusion Time Constant," *Journal of Energy and Power Technology* 2 (2020): 1–21.

23. I. Franzetti, A. Pushkarev, A.-L. Chan, and T. Smolinka, "Parasitic Effects in Impedance Spectrum of PEM Water Electrolysis Cells: Case Study of High-Frequency Inductive Effects," *Energy Technology* 11 (2023): 2300375.

24. D. Schmal, J. Van Erkel, and P. J. Van Duin, "Mass Transfer at Carbon Fibre Electrodes," *Journal of Applied Electrochemistry* 16 (1986): 422–430.

25. M. Becker and T. Turek, "New Mass Transport Correlation for Vanadium Redox-Flow Batteries Based on a Model-Assisted Parameter Estimation," *Batteries* 9 (2023): 253.

26. X. You, Q. Ye, and P. Cheng, "The Dependence of Mass Transfer Coefficient on the Electrolyte Velocity in Carbon Felt Electrodes: Determination and Validation," *Journal of the Electrochemical Society* 164 (2017): E3386–E3394.

27. Y. Chen, Z. Xu, C. Wang, et al., "Analytical Modeling for Redox Flow Battery Design," *Journal of Power Sources* 482 (2021): 228817.

28. M. Adamič, S. D. Talian, A. R. Sinigoj, I. Humar, J. Moškon, and M. Gaberšček, "A Transmission Line Model of Electrochemical Cell's Impedance: Case Study on a Li-S System," *Journal of the Electrochemical Society* 166 (2019): A5045–A5053.

Appendix A

Diffusion Layer Thickness for Flat Electrodes With Area $\mathbf{A = L \times w}$

If on the scale of diffusion, electrodes can be considered flat (with Nernst diffusion layer thickness smaller than electrode curvature) the following derivation can give important illustration of the system. In this strongly simplified model system we consider steady laminar Poiseuille flow between two parallel plates (separation h, mean velocity $\overline{u}$). The wall shear rate is

$$\gamma = \left.\frac{du}{dy}\right|_{\text{wall}} = \frac{6\overline{u}}{h}$$

Local diffusion layer thickness

From the Leveque approximation for the convection-diffusion equation, the local mass-transfer coefficient is

$$k(x) = 0.538\, D^{2/3}\, \gamma^{1/3}\, x^{-1/3}$$

where D is the diffusivity and x is the streamwise distance from the channel entrance. Defining the Nernst diffusion layer thickness by $k(x) = \frac{D}{\delta_N(x)}$ gives

$$\delta_N(x) = \frac{D}{k(x)} = 1.857 \left(\frac{Dx}{\gamma}\right)^{1/3}$$

Substituting $\gamma = 6\overline{u}/h$:

$$\delta_N(x) = 1.02 \left(\frac{Dxh}{\overline{u}}\right)^{1/3}$$

In terms of the volumetric flux per unit width, $q = \overline{u}h$, this becomes

$$\delta_N(x) = 1.02 \left(\frac{Dxh^2}{q}\right)^{1/3}$$

Now, we express the flow in terms of the total volumetric flow rate Q. The cross-sectional area for flow is $h \times w$, so

$$Q = \overline{u} \times (hw) = (\overline{u}h)w = qw$$

Thus, $q = Q/W$. Substituting into the expression for $\delta_N(x)$:

$$\delta_N(x) = 1.02 \left(\frac{Dxh^2w}{Q}\right)^{1/3}$$

Average diffusion layer thickness over length *L*

The average mass-transfer coefficient is defined by

$$k_{\text{avg}} = \frac{1}{L} \int_0^L k(x)\, dx$$

Substituting the local expression for $k(x)$:

$$k_{\text{avg}} = \frac{1}{L} \int_0^L 0.538\, D^{2/3} \gamma^{1/3} x^{-1/3}\, dx$$

Carrying out the integral:

$$k_{\text{avg}} = 0.807\, D^{2/3} \gamma^{1/3} L^{-1/3}$$

Thus, the average diffusion layer thickness is

$$\delta_{\text{avg}} = \frac{D}{k_{\text{avg}}} = 1.238 \left(\frac{DL}{\gamma}\right)^{1/3}$$

With $\gamma = 6\overline{u}/h$,

$$\delta_{\text{avg}} = 0.681 \left(\frac{DLh}{\overline{u}}\right)^{1/3}$$

In terms of volumetric flux per unit width $q = Uh$,

$$\delta_{\text{avg}} = 0.681 \left(\frac{DLh^2}{q}\right)^{1/3}$$

Substituting $q = Q/w$:

$$\delta_{\text{avg}} = 0.681 \left(\frac{DLh^2w}{Q}\right)^{1/3}$$

Appendix B

The Reynolds Number (Re) and the Schmidt Number (Sc)

$$\text{Re} = \frac{\rho \overline{u} d_f}{\mu}$$

$$\text{Sc} = \frac{\mu}{\rho D}$$

Here ρ is the electrolyte density, μ the dynamic viscosity, and $\overline{u}$ the mean velocity (flow rate divided by the cross-sectional area of the felt).